Observation of symmetrical reflection sidebands in a silica suspended-core fiber Bragg grating

M. L. V. Tse,[1,*] K. M. Chung,[1] L. Dong,[2] B. K. Thomas,[2] L. B. Fu,[2] K. C. D. Cheng,[1] C. Lu,[3] and H. Y. Tam[1]

[1]*Photonics Research Centre, Department of Electrical Engineering, The Hong Kong Polytechnic University, Hung Hom, Kowloon, Hong Kong SAR, China*
[2]*IMRA America Incorporation, 1044 Woodridge Avenue, Ann Arbor, Michigan 48105 USA*
[3]*Photonics Research Centre, Department of Electronics and Information Engineering, The Hong Kong Polytechnic University, Hung Hom, Kowloon, Hong Kong SAR, China*
*eemlvtse@inet.polyu.edu.hk

Abstract: We have observed symmetrical sidebands in reflection from Bragg grating written in a silica suspended-core fiber, which are caused by longitudinal periodic refractive index modulation in the Ge-doped suspended-core fiber with a core diameter of ~1.3 μm. Our simulation shows that the effective refractive index of the guided mode varied by 0.023% along the fiber with a period of ~650 μm. The periodic index variation can lead to amplitude modulation of fiber Bragg gratings, which can be studied by observing the spectra of a fiber Bragg grating written in the Ge-doped core. In addition, we have also characterized the temperature and strain responses of the fiber Bragg gratings, and showed that both responses in the suspended-core fiber are 20 to 25% lower than that of a fiber Bragg grating written on a conventional fiber.

OCIS codes: (060.2400) Fiber properties; (060.3735) Fiber Bragg gratings; (060.4005) Microstructured fiber; (060.4080) Modulation.

References and Links

1. J. K. Ranka, R. S. Windeler, and A. J. Stentz, "Visible continuum generation in air-silica microstructure optical fibers with anomalous dispersion at 800 nm," Opt. Lett. **25**(1), 25–27 (2000).
2. K. M. Kiang, K. Frampton, T. M. Monro, R. Moore, J. Tucknott, D. W. Hewak, D. J. Richardson, and H. N. Rutt, "Extruded single mode non-silica glass holey optical fibres," Electron. Lett. **38**(12), 546–547 (2002).
3. V. V. Kumar, A. K. George, J. C. Knight, and P. Russell, "Tellurite photonic crystal fiber," Opt. Express **11**(20), 2641–2645 (2003).
4. P. Petropoulos, H. Ebendorff-Heidepriem, V. Finazzi, R. C. Moore, K. Frampton, D. J. Richardson, and T. M. Monro, "Highly nonlinear and anomalously dispersive lead silicate glass holey fibers," Opt. Express **11**(26), 3568–3573 (2003).
5. H. Ebendorff-Heidepriem, P. Petropoulos, S. Asimakis, V. Finazzi, R. C. Moore, K. Frampton, F. Koizumi, D. J. Richardson, and T. M. Monro, "Bismuth glass holey fibers with high nonlinearity," Opt. Express **12**(21), 5082–5087 (2004).
6. K. Mukasa, M. N. Petrovich, F. Poletti, A. Webb, J. Hayes, A. van Brakel, R. A. Correa, L. Provost, J. Sahu, P. Petropoulos, and D. J. Richardson, "Novel fabrication method of highly nonlinear silica holey fibers," Optical Fiber Communications Conference, paper CMC535, Anaheim, California, March 2006.
7. L. Dong, B. K. Thomas, and L. B. Fu, "Highly nonlinear silica suspended core fibers," Opt. Express **16**(21), 16423–16430 (2008).
8. T. M. Monro, D. J. Richardson, and P. J. Bennett, "Developing holey fibres for evanescent field devices," Electron. Lett. **35**(14), 1188–1189 (1999).
9. A. S. Webb, F. Poletti, D. J. Richardson, and J. K. Sahu, "Suspended-core holey fiber for evanescent field sensing," Opt. Eng. **46**(1), 010503 (2007).
10. O. Frazão, S. H. Aref, J. M. Baptista, J. L. Santos, H. Latifi, F. Farahi, J. Kobelke, and K. Schuster, "Fabry–Pérot Cavity Based on a Suspended-Core Fiber for Strain and Temperature Measurement," IEEE Photon. Technol. Lett. **21**(17), 1229–1231 (2009).
11. L. B. Fu, B. K. Thomas, and L. Dong, "Efficient supercontinuum generations in silica suspended core fibers," Opt. Express **16**(24), 19629–19642 (2008).

12. M. C. Phan Huy, G. Laffont, V. Dewynter, P. Ferdinand, P. Roy, J. L. Auguste, D. Pagnoux, W. Blanc, and B. Dussardier, "Three-hole microstructured optical fiber for efficient fiber Bragg grating refractometer," Opt. Lett. **32**(16), 2390–2392 (2007).
13. P. A. Krug, R. Stolte, and R. Ulrich, "Measurement of index modulation along an optical fiber Bragg grating," Opt. Lett. **20**(17), 1767–1769 (1995).
14. D. Ramecourt, P. Bernage, P. Niay, M. Douay, and I. Riant, "Improvement in the measurement of index modulation along an optical fiber grating by movement of the probe spot perpendicularly to the fiber axis," Appl. Opt. **40**(34), 6166–6169 (2001).
15. M. L. V. Tse, H. Y. Tam, L. B. Fu, B. K. Thomas, L. Dong, C. Lu, and P. K. A. Wai, "Fusion splicing holey fibers and single-mode fibers: a simple method to reduce loss and increase strength," IEEE Photon. Technol. Lett. **21**(3), 164–166 (2009).
16. L. Labonte, D. Pagnoux, P. Roy, F. Bahloul, and M. Zghal, "Numerical and experimental analysis of the birefringence of large air fraction slightly unsymmetrical holey fibres," Opt. Commun. **262**(2), 180–187 (2006).
17. T. Erdogan, "Fiber grating spectra," J. Lightwave Technol. **15**(8), 1277–1294 (1997).
18. A. D. Kersey, M. A. Davis, H. J. Patrick, M. LeBlanc, K. P. Koo, C. G. Askins, M. A. Putnam, and E. J. Friebele, "Fiber grating sensors," J. Lightwave Technol. **15**(8), 1442–1463 (1997).
19. A. C. L. Wong, P. A. Childs, and G.-D. Peng, "Multiplexed fibre Fizeau interferometer and fibre Bragg grating sensor system for simultaneous measurement of quasi-static strain and temperature using discrete wavelet transform," Meas. Sci. Technol. **17**(2), 384–392 (2006).

1. Introduction

Microstructured suspended-core optical fibers [1] have been extensively reported in recent years. They consist of a solid core surrounded by 3 to 6 large air-holes in the cladding. The resultant fiber can exhibit extremely high nonlinearity due to a combination of very small core and the core materials used, and high NA. Core materials such as lead silicate [2], tellurite [3], lead silica [4], bismuth [5] silica [6] glasses, and more recently silica with Ge-doped core [7] have been used. In these fibers, the overlap between the holes and the optical field can be enhanced, therefore one of the key interests of such fiber is for evanescent-field based sensing [8], [9]. Strain and temperature sensing based on suspended-core fiber have also been demonstrated [10]. Due to the high nonlinearity, efficient supercontinuum generation is another important application [11].

By doping a suspended-core fiber with germanium, the fiber nonlinearity is enhanced, at the same time this also enables fiber Bragg grating (FBG) to be photo-written in the core [12]. New optical phenomena can be expected in a FBG written on an ultra-small-core fiber. In this paper, we report for the first time, the observation of amplitude modulation (AM) effect in a FBG that is most likely caused by a longitudinal core diameter variation. The main Bragg peak and a pair of symmetric sidebands were observed in the FBG reflection spectrum. We simulated the spectrum, from which, we deduced the period and the amplitude of the effective index variation, which is caused by the small longitudinal periodic core-size variation. A period of ~650 μm was found. It is difficult to directly measure the index modulation along a suspended-core fiber using the scattered light method [13], [14], because the air-holes introduce additional scattering. By studying the FBG-spectrum, the periodic index fluctuation is estimated to be of less than 0.03% along the fiber. This can be caused by a core-size variation of less than 0.2%.

The core-size variation is likely caused by an effect of several kHz in frequency, well beyond the bandwidth of the diameter feedback control loop. It may have its origin in instability of the drawing process at a mean pressure of 0.8 psi in the holes with feedback loop and at a drawing rate of ~155 m/min.

Since the temperature and the strain characteristics are important to any FBG sensors, we also presented the results of the responsivity for the FBG written on the suspended-core fiber. Comparisons have been made with FBG written on conventional fibers, and we found the responsivity for the FBG in the suspended-core fiber were lower than that of the conventional fibers in both cases. One potential application of these FBGs in suspended core fibers is acoustic sensors with an improved bandwidth of response.

2. Experiment and result

The suspended-core fiber used in the experiment has a core diameter of ~1.27 μm, NA~1 and fiber loss of ~78 dB/km [7]. The central ~60% of the core diameter is doped with graded index germanium with near parabolic profile. The outer diameter is 125 μm. The suspended-core fiber was connected to high NA fibers (Nufern-UHNA4) at both ends via strong fusion splicing [15]. This ensured the air-holes were sealed, allowing enough loaded hydrogen to be retained in the core for sufficient time during the FBG inscription [12]. The spliced fibers were left in a hydrogen chamber with pressure of 2000 psi for one month at room temperature. It should be noted that due to the small core size and its proximity to the air holes, if the holes were not sealed, the hydrogen would diffused out completely within a few minutes through the air holes once it is taken out of the chamber.

Figure 1 shows a schematic of the experimental setup of the FBG photo-written onto the hydrogen loaded Ge-doped suspended-core fiber with periodic diameter variation. A fiber Bragg grating with a length of 8 mm was inscribed onto the fiber. The general diameter of the core was found from the SEM cross-section image of the fiber, shown in the inset of Fig. 1.
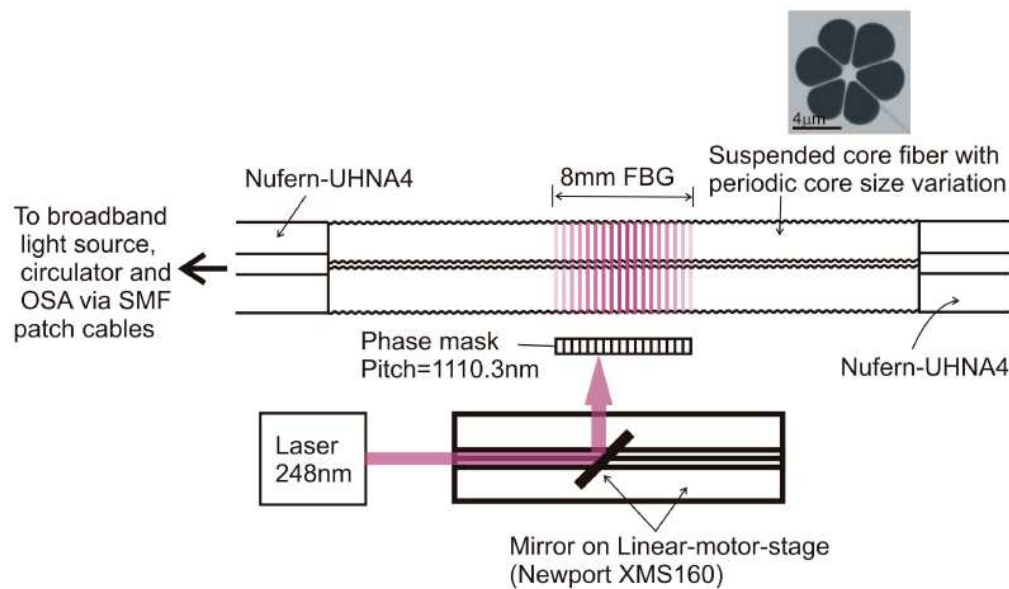

Fig. 1. A schematic of the experimental setup of the FBG photo-written onto the hydrogen loaded Ge-Doped suspended core fiber with periodic diameter variation. Inset: the SEM picture of the fiber's core-cladding region.

The FBG was photo-written by using the common technique of a phase mask in front of a fiber. A 248 nm KrF laser (BraggStar-200 from Tuilaser) with power of 12 mJ at 200 Hz was used for the inscription. The phase mask was made from Ibsen with pitch of 1110.3 nm, which produced a corresponding fiber grating with a period of 555.45 nm. A Hamming apodization profile was used for writing the grating. The profile was produced by controlling a linear-motor-stage (Newport XMS160) in 'jogging' mode to repeatedly scan the fiber grating region. Each scan took less than five seconds. In total, the grating was scanned six times, including three invert Hamming scans without using the phase mask. The purpose of the invert function scanning was to flatten the "DC" UV dose along the grating, and therefore, Bragg peaks with reduced noise were produced. After applying the apodization process, the side-lobes immediately adjacent to the Bragg peak reflection were suppressed to −18 dB. The reflection spectrum is shown in Fig. 2.
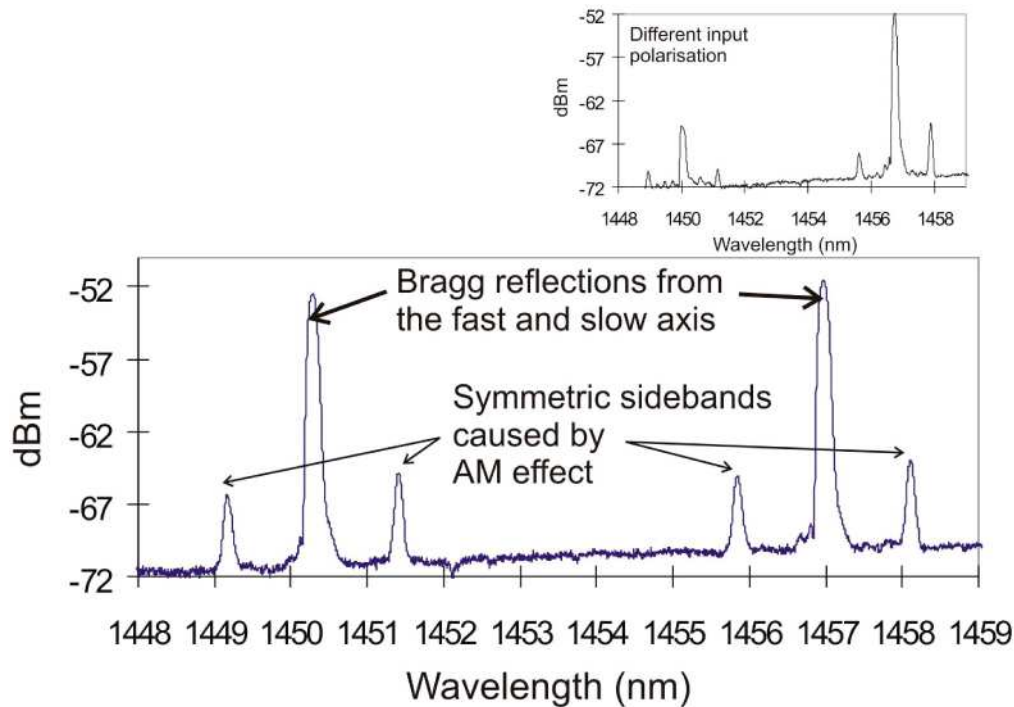
Fig. 2. The suspended core fiber FBG reflection spectrum measured by an OSA. *Inset*: one of the observed spectra when the input polarization is changed using a pair of fiber optic polarizers.

There were two Bragg peaks in the reflection spectrum, shown in Fig. 2. The two Bragg reflections were caused by the birefringence of the fiber, utilizing two polarization axes. An example of the reflection spectrum with different polarization of the input light is shown in the inset of Fig. 2. It shows that the relative amplitude of the Bragg peaks can be varied by varying the input polarization as expected. Very small fluctuations of the geometrical parameters in these small core fibers can also have a noticeable effect on the birefringence [16]. Fiber birefringence can derived from the wavelength separation of the FBGs for the two orthogonally polarized lights, giving a fiber birefringence of 0.0047, very close to the measured 0.0045 at 1020 nm [11]. In addition to the main Bragg peaks, there were also two symmetrical side peaks generated on each axis. The wavelength separation between the Bragg peak and the side peak was 1.245 nm. We have written a number of FBGs in this fiber showing similar sidebands. The same setup has also been used regularly in writing FBGs in other fibers. Such sidebands were never observed. The appearance of these symmetrical reflection sidebands was due to a periodic variation of the effective refractive index along the propagation axis of the fiber, most likely from a core diameter fluctuation. Since no higher order sidebands were observed, a sinusoidal modulation with a period of ~650 μm is expected from the sideband separation. Since we are confident that this is not from the writing setup, we suspect this is caused by the suspended core fiber. The air holes near the core may cause reflection of writing beams. For these spurious reflected beams to have any effect, multiple reflections are required. Even with the high index contrast of the glass-air interface, these reflected beams is expected to be at least four orders of magnitudes below the main beam after two reflections on defocusing cylindrical surface of the air holes. It is not expected to be any concern. Any fluctuations in the glass can also be ruled out, because this would imply a very unlikely high spatial variation in the preform (the germanium-doped preform is from J-Fiber, a well known commercial supplier). Since the fibers were drawn at speed exceeding

100 m/min, such fluctuations can only by caused by effect at over 1 KHz. The frequency of the fluctuations is much higher than most drawing-related process. The air holes are pressurized during the draw. It is possible that an instability in the air-pressure control in the small holes may lead to air hole size fluctuations. To prove the index modulation hypothesis, we simulated the spectral response, and the result is presented in the next section.

3. Simulation and discussions

For comparison, we simulated the spectra for a conventional fiber with a constant effective index and for the suspended-core fiber with a periodic varying effective index profile by using the well known transfer matrix given in [17]. The transfer matrix is used in conventional grating simulation to model a non-uniform reflection grating. The "DC" effective refractive index profiles we used for our simulation are shown in Fig. 3(i). The reference apodization profile is shown in Fig. 3(ii). Here, we only simulated the spectra at the wavelength region at the slow axis. The effective index was estimated using the following expression:

$$\lambda_B = 2n_{eff}\Lambda, \tag{1}$$

where λ_B is the Bragg wavelength, n_{eff} is the average effective refractive index of the grating and Λ is the grating period. A constant effective index of 1.3120 was calculated using Eq. (1) and was used in the simulations for the conventional fiber. It should be noted that the effective index is much lower than that of the silica glass, indicating that a large part of the light propagates in the air.

The relationship between the wavelength separation of the symmetrical side peaks and the fluctuation period is given by the following Fabry–Pérot interference equation in FBG:

$$\Delta\lambda = \frac{\lambda_B^2}{2n_{eff}P} \tag{2}$$

where P is the period of the "DC" refractive index modulation and $\Delta\lambda$ is the wavelength separation between the Bragg peak and the side peaks. From the experimental spectrum, $\Delta\lambda = 1.245$ nm and $\lambda_B = 1456.9$ nm, therefore from Eq. (2), $P\sim650$ µm. A sinusoidal refractive index profile with period of 650 µm and the effective index of 1.3120 ± 0.0003 was used in the simulations for the suspended-core fiber. The simulated results are shown in Fig. 3(iii). The simulated reflection spectrum for the suspended-core fiber agreed very well with that of the experiment, see Fig. 3(iv).
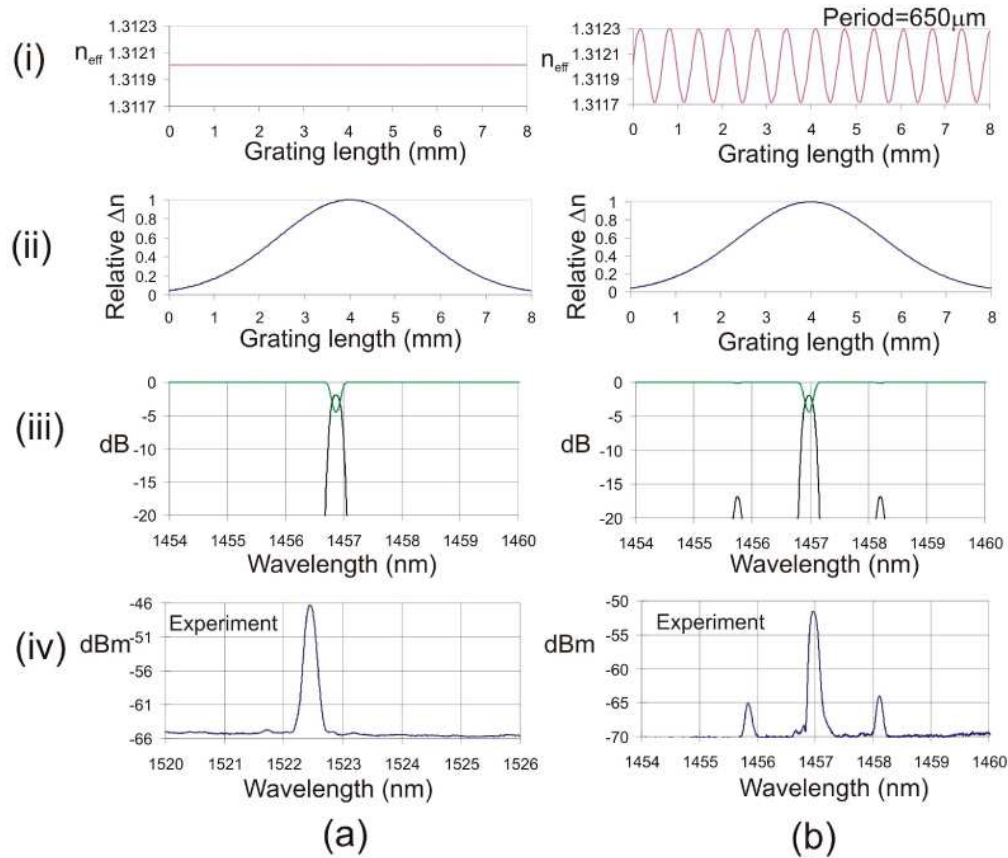
Fig. 3. Simulated spectra of (a) a FBG written on a conventional single-mode fiber with constant effective index along the fiber length, and (b) the suspended core fiber with a periodic effective index profile. (i) Shows the effective index profile of the two fibers. (ii) The apodization profile used for both fibers. (iii) The simulated spectra of the slow axis. (iv) The reflection spectra observed in the experiment with the same setup.

As discussed above, the most likely caused of the index variation was by a periodic core or structure size variation. Therefore, we investigated the amount of size variation of the diameter along the fiber. First, we matched the amplitude of the peaks of the simulated and experimental spectra to obtain the refractive index variation, Δn_{eff}, assuming the core diameter is sinusoidally modulated along the entire grating length. Here, the amplitude difference between the main Bragg peak and the side peaks was ~13 dB, correspond to Δn_{eff} of ± 0.0003 that was used in the simulation, see Fig. 3(b,i). Next, we simulated the fiber with the newly found Δn_{eff} by a finite-element-method using Comsol FEMLAB to find the amount of variation of the core diameter. The outline of the fiber structure was taken directly from the SEM image. The simulated structure consisted of a core doped with germanium in the center with diameter of 60% of the effective core diameter. Since the exact dopant profile was unknown, a step index profile with a step of 0.025 was used in the simulation. A grid of 30019, 0.036 μm triangular mesh elements was used in the simulation. Figure 4 shows the changes in effective index as the whole structure was scaled in size. We found that if the core-diameter varied ± 0.16% (± 2 nm), the corresponding effective index Δn varied ± 0.023% (± 0.0003).
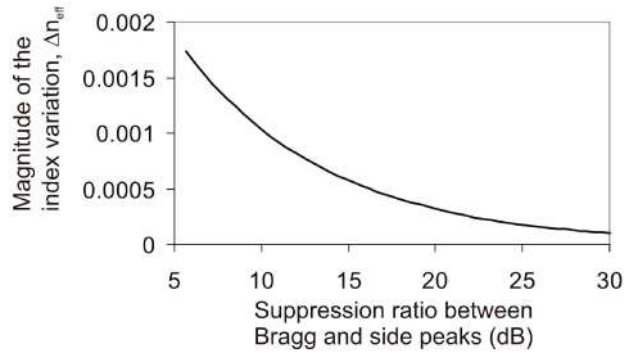
Fig. 4. A graph to show the change in effective index as the whole structure was scaled in size.

We have demonstrated that the AM effect from a nano-scale core-size variation of a suspended-core fiber can be observed in the FBG reflection spectrum. Symmetric sidebands were generated with extremely small variation in core diameter. The wavelength separation between the Bragg peak and the side peaks determines the period of the index, or hence the corresponding period of the core-size fluctuation along the fiber. The magnitude of the index or core diameter variation is proportional to the amplitude of the side peaks relative to the Bragg peak. Figure 5 shows that as the suppression ratio between the peaks increases, the magnitude of the index variation decreases.
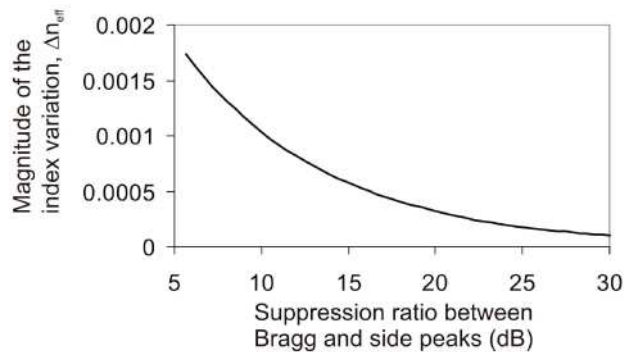

Fig. 5. A graph to show the amplitude difference between the Bragg and side peaks.

The effect was not observed previously in conventional or other microsturctured fibers. The drawing instability at the origin of the effect may need a combination of large air holes next to the core, thin webs and small core. Further study is required for a better understanding of the effect.

4. Temperature and Strain response of the FBG

In this section, we investigate the temperature and strain characteristics of the FBG written on the suspended-core fiber. A 10 mm long U-shape heater was used to heat up the 8 mm long FBG. The reflection spectra were recorded for every 10 °C from 20 °C to 130 °C. The responses were similar for both axes, the resultant spectra for the slow axis are shown in Fig. 6(a), and the wavelengths for the three peaks at different temperature are shown in Fig. 6(b). Figure 6 shows that the peaks shift to longer wavelengths as the temperature increases, with the thermal responsivity of ~7.2 pm °C^{-1} at 1457 nm with constant strain. The relationship between the thermal responsivity and Bragg wavelength of a FBG in a conventional fiber is given as [18]:

$$\frac{1}{\lambda_B}\frac{\delta\lambda_B}{\delta T}=6.67\times10^{-6}\,{}^{o}C^{-1}, \tag{3}$$

where δL_B is the wavelength shift, δT is the change in temperature and λ_B is the Bragg wavelength. From Eq. (3), the thermal responsivity of a FBG in a conventional fiber is calculated to be ~9.72 pm °C^{-1} at 1457 nm. In comparison, the thermal responsivity of the FBG written on the suspended-core fiber was ~25% lower than that of the FBG in a conventional fiber. The lower response is expected because the suspended-core fiber is a heterogeneous structure, in which the field spreads in both silica and air (the index remains quasi constant with temperature). Therefore, the effective index of the guided mode in this fiber is less sensitive to changes in the temperature than the effective index of the corresponding mode in a standard fiber.
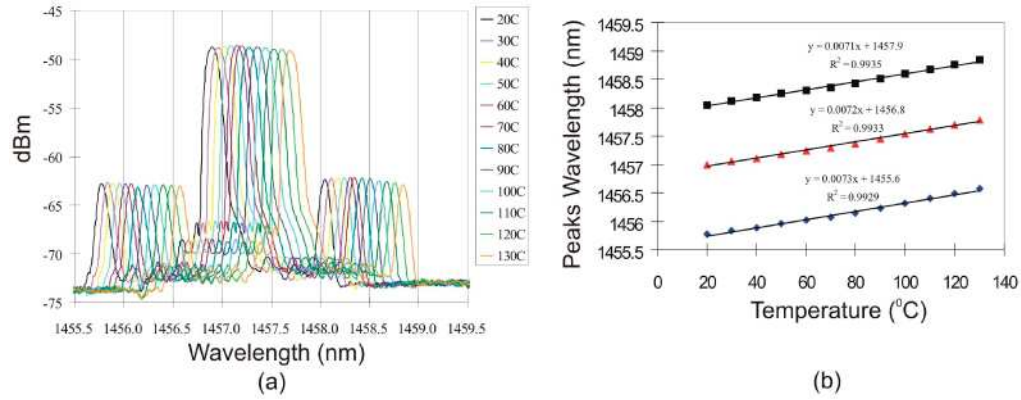

Fig. 6. (a) The FBG reflection spectra of the suspended core fiber at different temperature at the slow axis. (b) The maxima of the three peaks at different temperature.

The strain responses of the FBGs written on a conventional fiber and the suspended core fiber were characterized by the suspended weight method [19]. The same phase mask was used to produce the FBG in both fibers; therefore the Bragg reflections appeared at different wavelengths. Figure 7 shows the strain responsivity of the two cases. It is shown with the scale in weight directly in unit of grams instead of mirco-strain (με) that is used conventionally. Figure 7 shows that the peaks shift to longer wavelengths as the strain increases. The strain responsivity of the suspended-core FBG was ~9.9 pm g^{-1} at 1457 nm with constant temperature. The conversion from weight to micro-strain was given for conventional fiber that has solid core and cladding, however, for fiber with air-holes cladding, it is more difficult to do the conversion accurately. Nevertheless, a comparison between the conventional case and the suspended-core case is still possible by using the following conventional relations of the strain responsivity and the Bragg wavelength [18]:

$$\frac{1}{\lambda_B}\frac{\delta\lambda_B}{\delta\varepsilon}=0.78\times10^{-6}\,\mu\varepsilon^{-1}, \tag{4}$$

where $\delta\varepsilon$ is the change in the applied strain. The strain responsivity of a FBG in a conventional fiber is ~1.14 pm με^{-1} at 1457 nm, taking 1 g = 11.07 με [19], the strain responsivity is ~12.6 pm g^{-1} at 1457 nm. In comparison, the strain responsivity of the FBG written on the suspended-core fiber is ~20% lower than that of the FBG in a conventional fiber. Again, this may due to the small core isolated by a high air-fill cladding and held by very thin silica bridges to connect to a thick silica outer wall.
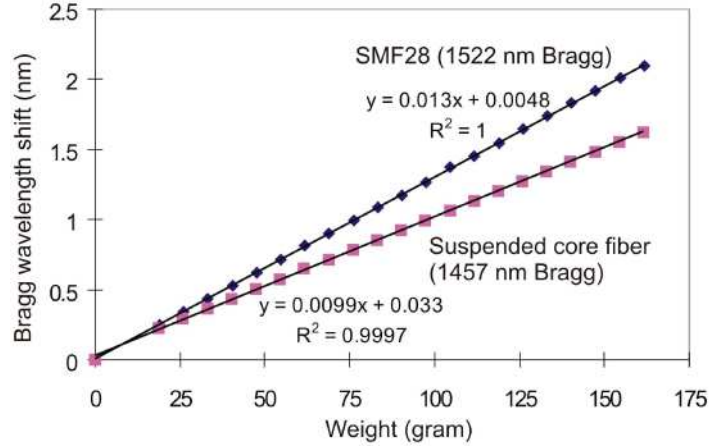
Fig. 7. The strain response of the FBG written on the suspended-core fiber and a conventional fiber using the same phase mask. Note the difference in the Bragg wavelength and the strain scale is presented in weight.

By rewriting Eq. (4), we get:

$$\frac{\delta\lambda_B}{\lambda_B} = 0.78 \frac{w}{AE}, \qquad (5)$$

where w is the weight, A is the cross-sectional area of the fiber and E is the Young's modulus. The cross-sectional area of the suspended-core fiber is smaller than that of a conventional fiber. Equation (5) shows that if A decreases, $\delta\lambda_B/\delta w$ would increase. The measured smaller slope indicates that the thin webs are able to transfer about 77% of the stress to the small core.

5. Conclusions

We have reported for the first time, the observation of the amplitude modulation effect in a fiber Bragg grating written on a suspended core fiber. The effect was caused by a periodic effective index fluctuation. The period and the magnitude of the fluctuation can be determined by studying the separation and the amplitude difference of the main peak and the side peaks in the reflection spectrum respectively.

The temperature and the strain responses of the FBG have been characterized. It was found that the responsivities for the suspended-core FBG were lower than that of the conventional FBG.

Acknowledgment